

# CONSTRAINING FUNDAMENTAL PHYSICS WITH THE COSMIC MICROWAVE BACKGROUND\*

Anthony Challinor<sup>†</sup>

<sup>1</sup> Astrophysics Group, Cavendish Laboratory, J. J. Thomson Avenue,  
Cambridge, CB3 0HE, UK

## Abstract

The temperature anisotropies and polarization of the cosmic microwave background (CMB) radiation provide a window back to the physics of the early universe. They encode the nature of the initial fluctuations and so can reveal much about the physical mechanism that led to their generation. In this contribution we review what we have learnt so far about early-universe physics from CMB observations, and what we hope to learn with a new generation of high-sensitivity, polarization-capable instruments.

Key-words: cosmic microwave background — early universe

## 1. Introduction

The cosmic microwave background (CMB) radiation has an almost perfect black-body spectrum with mean temperature 2.725 K (Mather et al 1994). Once corrected for a kinematic dipole due to our motion, the CMB is remarkably isotropic with fluctuations at the  $10^{-5}$  level. These were first detected by the COBE satellite in 1992 (Smoot et al 1992) and have now been measured over three decades of scale by a combination of ground-based and balloon-borne experiments and the WMAP satellite (Bennett et al 2003). CMB photons were tightly coupled to matter in the early universe but propagated essentially freely after the primordial plasma recombined to form neutral atoms<sup>1</sup>. For this reason, the CMB provides a snapshot of the spatial fluctuations on a spherical shell of comoving radius 14000 Mpc at redshift  $z \sim 1000$  when the universe was only  $400 \times 10^3$  years old. The small amplitude of these fluctuations [ $O(10^{-5})$ ] means they are well described by linear perturbation theory and the physics of the CMB is thus very well understood.

---

\*Presented at the *Workshop on Cosmology and Gravitational Physics*, 15–16 December 2005, Thessaloniki, Hellas (Greece), *Editor*: N. K. Spyrou.

<sup>†</sup>a.d.challinor@mrao.cam.ac.uk

<sup>1</sup>Recent WMAP3 results indicate that around 10% of the photons re-scattered once the universe reionized around redshift 10.

The fluctuations on the last-scattering surface are believed to have resulted from primordial curvature fluctuations plausibly generated quantum mechanically during an inflationary phase in the first  $10^{-35}$  seconds. These primordial fluctuations are processed by gravitational instability and, on smaller scales, by the acoustic physics of the plasma which is supported by photon pressure. This makes the CMB anisotropy sensitive to the physics that initially produced the fluctuations and to the composition of the matter in the universe which affects the acoustic physics.

In this *contribution* we review what we have learnt from current CMB observations, with particular emphasis placed on constraints on fundamental physics and models of the early universe. We also look forward briefly to what might be learnt with more sensitive future observations, such as tighter constraints on the gravitational wave background predicted from inflation and sub-eV constraints on neutrino masses from weak gravitational lensing of the CMB.

## 2. CMB Physics

We begin with a brief review of the physics of the CMB temperature and polarization anisotropies. For more complete reviews see e.g. Hu & Dodelson (2001), Hu (2002) and Challinor (2005).

Consider a spatially-flat background universe linearly perturbed by density perturbations and gravitational waves. The metric can be taken to be  $ds^2 = a^2(\eta)\{(1 + 2\psi)d\eta^2 - [(1 - 2\phi)\delta_{ij} + h_{ij}]dx^i dx^j\}$ , where the Newtonian-like potentials  $\psi$  and  $\phi$  describe the scalar (density) perturbations and the transverse, trace-free  $h_{ij}$  describes tensor perturbations (gravitational waves). In the absence of anisotropic stresses  $\phi = \psi$ . If we ignore scattering after the universe reionized, and approximate the last-scattering surface as sharp, the fractional temperature fluctuation along a line of sight  $\hat{\mathbf{n}}$  has a scalar contribution

$$\Theta(\hat{\mathbf{n}}) = \Theta_0|_E + \psi|_E - \hat{\mathbf{n}} \cdot \mathbf{v}_b|_E + \int_E^R (\dot{\psi} + \dot{\phi}) d\eta, \quad (1)$$

and a tensor contribution

$$\Theta(\hat{\mathbf{n}}) = -\frac{1}{2} \int_E^R \dot{h}_{ij} \hat{n}^i \hat{n}^j d\eta. \quad (2)$$

Here, an overdot denotes a derivative with respect to conformal time  $\eta$ . Performing a spherical harmonic expansion of the anisotropies,

$$\Theta(\hat{\mathbf{n}}) = \sum_{lm} a_{lm} Y_{lm}(\hat{\mathbf{n}}), \quad (3)$$

the power spectrum is defined by  $\langle a_{lm} a_{l'm'}^* \rangle = C_l^T \delta_{ll'} \delta_{mm'}$  where the angle brackets denote an ensemble average (or quantum expectation value). This form of the correlator follows from statistical isotropy and homogeneity. The quantity  $l(l+1)C_l^T/2\pi$  is usually plotted and this gives the contribution to the mean-square anisotropy per  $\ln l$ .

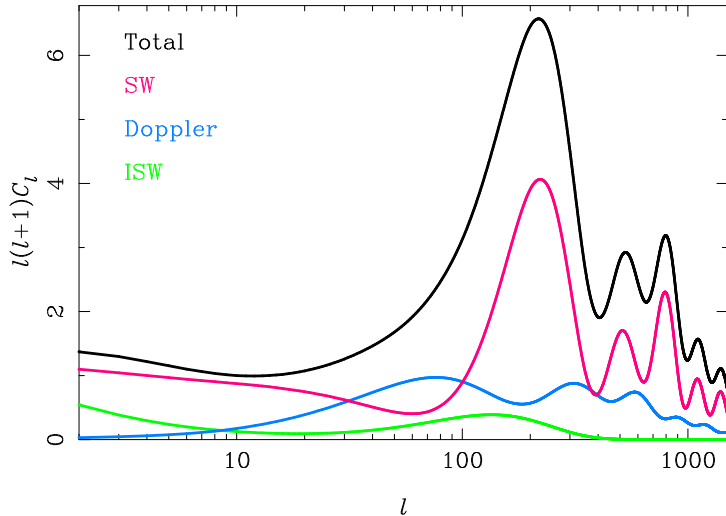


Figure 1. Scalar contributions to the temperature power spectrum from scale-invariant adiabatic initial fluctuations. At high  $l$  the contributions are (from top to bottom): total power (black); Sachs-Wolfe (magenta); Doppler (blue); and the integrated Sachs-Wolfe effect (green).

The scalar anisotropies, equation (1), are sourced by fluctuations on the last-scattering surface at position  $E$  and an integral along the line of sight involving the evolution of the Weyl potential  $\psi + \phi$ . Regions of photon over-density have a positive intrinsic temperature fluctuation  $\Theta_0$ , but this is modified by the local gravitational potential  $\psi|_E$  that the photon must climb out of at last scattering to give the observed anisotropy. There is a further contribution from the baryon peculiar velocity  $\mathbf{v}_b$  at the last-scattering event which Doppler blueshifts photons that scatter along the direction of motion. The last ‘integrated Sachs-Wolfe’ (ISW) term in equation (1) contributes to the large-angle fluctuations because of the decay of the gravitational potentials once dark energy dominates the expansion, and also on smaller scales due to evolution of the potentials around last scattering before the universe is fully matter dominated. The various contributions to the anisotropy power spectrum from scalar perturbations are shown in Fig. 1 for *adiabatic initial conditions* where the *relative* composition of the universe is initially the same everywhere. Such initial conditions are natural in inflation models with only a single field, but in models with multiple fields the initial conditions may include an *isocurvature* component where the relative composition fluctuates in space in such a way as not to perturb the curvature.

The initial curvature fluctuations are processed by gravitational and acoustic physics to determine the fluctuations on the last scattering surface. In particular, on scales above the photon mean free path, the radiation and baryons are tightly-coupled and the radiation is isotropic in the plasma rest-frame. In this limit, the intrinsic temperature fluctuation satisfies an oscillator equation (Hu & Sugiyama 1995)

$$\ddot{\Theta}_0 + \frac{\mathcal{H}R}{1+R}\dot{\Theta}_0 - \frac{1}{3(1+R)}\nabla^2\Theta_0 = 4\ddot{\phi} + \frac{4\mathcal{H}R}{1+R}\dot{\phi} + \frac{4}{3}\nabla^2\psi, \quad (4)$$

where  $\mathcal{H} \equiv \dot{a}/a$  is the conformal Hubble parameter and  $R \equiv 3\rho_b/(4\rho_\gamma)$  is the ratio of baryon to photon density. The sound speed in the plasma is  $c_s^2 = 1/[3(1+R)]$  and is reduced from the value for a photon gas by the inertia of baryons. The oscillator is damped by the Hubble drag on the baryons<sup>2</sup> and is driven by the gravitational potentials. A potential well accretes surrounding plasma until the induced pressure gradients balance the gravitational force. At this point  $\Theta_0 = -(1+R)\psi$  (ignoring evolution of the gravitational potentials) but the plasma is still infalling and doesn't turn around until a higher density. The amplitude of the oscillation about the midpoint is determined by the initial conditions and gravitational driving; for adiabatic initial conditions the plasma starts off over-dense in potential wells with  $\Theta_0 = -\psi(0)/2$  for all wavelengths. This means that the oscillations of different Fourier modes all start off in phase, at an extrema, but the period of their subsequent oscillation is wavelength dependent. It follows that at the last-scattering surface different wavelengths will be caught at different phases of a cosine-like oscillation. Those wavelengths at an extremum at last scattering will give rise to a peak in the anisotropy power spectrum at a multipole  $l \sim kd_A(r_*)$ , where  $d_A(r_*)$  is the angular-diameter distance back to last scattering at comoving distance  $r_* \approx 14$  Gpc.

The tensor anisotropies, equation (2), involve an integral of the metric shear  $\dot{h}_{ij}$  which describes the local anisotropy in the expansion of the universe due to the presence of gravitational waves: CMB photons experience line-of-sight-dependent redshifts that imprint temperature anisotropies on the microwave sky. A cosmological background of gravitational waves is naturally produced during inflation from the vacuum fluctuations in the massless field  $h_{ij}$  (Starobinskii 1979); see Sec. 5. On scales larger than the Hubble radius,  $h_{ij}$  is constant but once a mode enters the Hubble radius it starts to oscillate with an amplitude that decays as  $a^{-1}$ . On scales  $\lesssim 3^\circ$ , i.e.  $l \gtrsim 60$ , the relevant gravitational waves at any distance back to last scattering are sub-Hubble and so the tensor signal is only appreciable on scales larger than this.

## 2.1 CMB Polarization

The other important CMB observable is its linear polarization (Rees 1968). The tightly-coupled description of the plasma given above breaks down for short wavelength modes, and universally as the mean-free path grows around recombination. As photons start to diffuse out of over-dense regions their density and velocity perturbations are damped which leads to an exponential damping tail in the anisotropy power spectrum (Silk 1968). However, a quadrupole anisotropy also starts to develop in the radiation and subsequent Thomson scattering generates linear polarization with an r.m.s.  $\sim 5 \mu\text{K}$ .

Linear polarization is described by Stokes parameters  $Q$  and  $U$  which measure the difference in intensity between two orthogonal polarizers ( $Q$ ) and the same rotated by  $45^\circ$ . The Stokes parameters form the components of the polarization tensor

---

<sup>2</sup>Expansion redshifts away the peculiar velocity of matter.

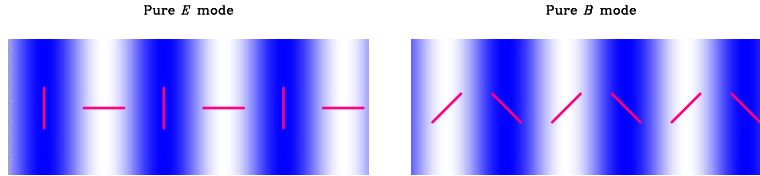


Figure 2. Polarization patterns for a pure  $E$  mode (left) and  $B$  mode (right) for a single Fourier mode on a flat patch of sky. In the basis defined by the wavevector, the  $E$  mode has vanishing  $U$  and the  $B$  mode vanishing  $Q$ .

$\mathcal{P}$  which measures the (zero-lag) correlation of the electric field components in the radiation. They are therefore basis dependent but coordinate-independent fields can be derived by writing  $\mathcal{P}$  as a gradient (or electric) part and curl (or magnetic) part (Kamionkowski, Kosowsky & Stebbins 1996; Zaldarriaga & Seljak 1996):

$$\mathcal{P}_{ab}(\hat{\mathbf{n}}) = \sum_{lm} \sqrt{\frac{(l-2)!}{(l+2)!}} \left( E_{lm} \nabla_{\langle a} \nabla_{b \rangle} Y_{lm}(\hat{\mathbf{n}}) + B_{lm} \epsilon^c{}_{\langle a} \nabla_{b \rangle} \nabla_c Y_{lm}(\hat{\mathbf{n}}) \right). \quad (5)$$

Here, the covariant derivatives are in the surface of the unit (celestial) sphere, angle brackets denote the symmetric, trace-free part and we have expanded the electric and magnetic parts in spherical harmonics. By way of example, Fig. 2 shows the polarization patterns for  $E$  and  $B$  modes that are locally plane waves. The  $E$  field behaves as a scalar under parity transformations but  $B$  is a pseudo-scalar. If parity-invariance is respected in the mean, there are only three additional non-vanishing power spectra: the  $E$ - and  $B$ -mode auto-correlations,  $C_l^E$  and  $C_l^B$ , and the cross-correlation of  $E$  with the temperature anisotropies  $C_l^{TE}$ . For linear scalar perturbations the  $B$ -mode polarization vanishes by symmetry, but gravitational waves produce  $E$  and  $B$  modes with approximately equal power (Kamionkowski et al 1996; Zaldarriaga & Seljak 1996; Hu & White 1997). This makes the large-angle  $B$  mode of polarization an excellent probe of primordial gravitational waves and several groups are now developing instruments with the aim of searching for this signal; see Sec. 6.

The temperature and polarization power spectra from density perturbations and gravitational waves are compared in Fig. 3. The gravitational wave amplitude is set to a value close to the current upper limit from the temperature anisotropies. Note that for scalar perturbations,  $C_l^E$  peaks at the troughs of  $C_l^T$  since the radiation quadrupole at last scattering is derived mostly from the plasma bulk velocity which oscillates  $\pi/2$  out of phase with the intrinsic temperature. The polarization from density perturbations is maximised around  $l \sim 1000$  which is related to the angle subtended by the photon mean-free patch around recombination. The ‘bump’ in the polarization spectra on large angles is due to reionization (Zaldarriaga 1997). Once the ultraviolet light from the first compact objects has reionized the intergalactic medium, the liberated electrons can re-scatter the CMB. This has the effect of damping the temperature and polarization spectra by  $e^{-2\tau}$ , where  $\tau$  is the optical depth to Thomson scattering, on scales inside the horizon at that epoch. However, Thomson scattering of the quadrupole anisotropy that has now developed in the free-streaming radiation produces new large-angle polarization. The power in the

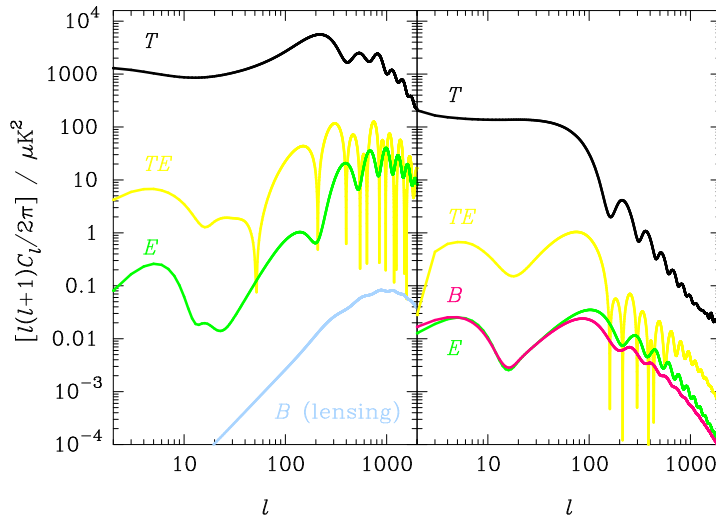


Figure 3. CMB temperature and polarization power spectra from scalar (left) and tensor perturbations (right) for a tensor-to-scalar ratio  $r = 0.38$ . The  $B$ -mode power generated by weak gravitational lensing is also shown.

reionization bump scales like  $\tau^2$  and the angular scale is related to the epoch of reionization. The high value  $\tau = 0.17$  adopted in Fig. 3, favoured by the first-year WMAP data (Kogut et al 2003), is now at odds with the recent three-year WMAP data (Page et al 2006); see Sec. 4. Also shown in the figure is the non-linear  $B$ -mode signal generated by weak gravitational lensing of the primary  $E$ -mode polarization from density perturbations (Zaldarriaga & Seljak 1998; Lewis & Challinor 2006). We discuss this signal further in Sec. 6.

### 3. Current Observational Situation

Imaging the CMB temperature anisotropies is now a mature field. A number of complementary technologies have been deployed to map the CMB from frequencies of a few tens to hundreds of GHz. The remarkable full-sky maps from the WMAP satellite, most recently on the basis of three years of data (Hinshaw et al 2006), have a resolution up to 15 arcmin and are signal-dominated up to multipoles of a few hundred. The main cosmological information in the CMB images is encoded in their power spectra so in Fig. 4 we show a selection of recent measurements of the  $C_l^T$  taken from Jones et al (2005). The qualitative agreement with the theoretical expectation is striking, with the measurements clearly delimiting the first three acoustic peaks. As we discuss later, the agreement stands up to rigorous statistical analysis and has provided a very powerful means of constraining cosmological parameters and models. While the community awaits the high-sensitivity, full-sky results from the Planck satellite, due for launch in 2008, a number of groups are working to improve on ground-based measurements of the small angular scales inaccessible to WMAP.

Polarization measurements are less mature, with the first detection reported by

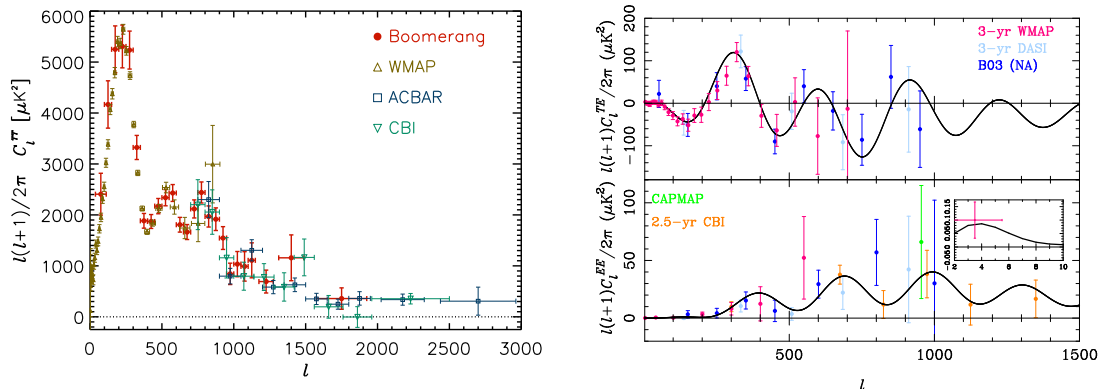


Figure 4. Recent CMB temperature (left) and polarization (right;  $C_l^{TE}$  top and  $C_l^E$  bottom) power spectra measurements. For polarization all measurements are plotted including WMAP3. The solid lines in the polarization plots are the theoretical expectation on the basis of the temperature data and an optical depth  $\tau = 0.08$ . The temperature plot, from Jones et al (2005), shows results from WMAP1 and a selection of ground and balloon-borne instruments. The recent WMAP3 data helps delimit the third acoustic peak in  $C_l^T$  further.

DASI in 2002. Since that first detection, four further groups have published detections of  $E$ -mode polarization through its auto-correlation  $C_l^E$ . These measurements, also shown in Fig. 4, are still very noisy, but the qualitative agreement with the best-fit model to the temperature spectrum is striking. The cross-correlation  $C_l^{TE}$  has also been measured by several of these groups, and with the arrival of the third-year WMAP data the measurements are now quite precise for  $l \lesssim 200$ . As we discuss further in Sec. 6, several new high-sensitivity polarization-capable experiments are currently under construction and these have the ambition of measuring the  $B$ -mode power spectrum. At present only upper limits exist for  $C_l^B$ ; see Fig. 6. These instruments will also significantly improve on current measurements of  $C_l^E$ .

## 4. Major CMB Milestones and their Cosmological Implications

The current CMB data has confirmed a number of bold theoretical predictions, some of which pre-date the data by over thirty years. In this section we briefly describe these major milestones and discuss their implications for constraining the cosmological model.

### 4.1 Sachs-Wolfe Plateau and the Late-time ISW Effect

The large-angle temperature anisotropies are dominated by the Sachs-Wolfe effect,  $\Theta_0 + \psi$ , and the ISW effect (Sachs & Wolfe 1967). For adiabatic initial conditions, the combination  $\Theta_0 + \psi$  reduces to  $\psi/3$  on scales above the sound horizon at last scattering and so potential wells appear as cold regions. For a nearly scale-invariant spectrum of primordial curvature perturbations, we should

have  $l(l+1)C_l^T \approx \text{const.}$  on such scales. This plateau was first seen in the COBE data (Hinshaw et al 1996), and has since been impressively verified by WMAP. Departures from scale-invariance imply a slope to the  $l(l+1)C_l^T$  spectrum on large scales and this can be used to help constrain the spectral index  $n_s$  of the primordial spectrum; see Sec. 5. In practice, the large-angle data is not very constraining due to the large cosmic variance there, i.e. the fact we only have access to a sample of  $2l+1$  spherical harmonic modes at each  $l$  with which to estimate the variance of their population,  $C_l^T$ .

The late-time ISW effect, from the decay of the Weyl potential  $\phi + \psi$  as dark energy dominates, contributes significantly on the largest angular scales. It is suppressed on smaller scales due to peak-trough cancellation in the integral along the line of sight and from the decay of the potential on sub-horizon scales during radiation domination. The late-time ISW adds incoherently with the Sachs-Wolfe contribution since at a give  $l$  they probe different linear scales. It is the only way to probe late-time growth of structure with linear CMB anisotropies (see Sec. 7 for an example of a non-linear probe), but this is hampered by large cosmic variance. The late-ISW effect produces a positive correlation between large-angle temperature fluctuations and tracers of the gravitational potential at redshifts  $z \lesssim 1$ . This was first detected by correlating the one-year WMAP data with the X-ray background and with the projected number density of radio galaxies (Boughn & Crittenden 2004), and has since been confirmed with several other tracers of large-scale structure. The correlation is sensitive to both the energy density in dark energy and any evolution with redshift. The ISW constraints on the former indicate  $\Omega_\Lambda \sim 0.8$ , consistent with other cosmological probes; see e.g. Cabre et al (2006). As yet there is no evidence for evolution but significant improvements can be expected from tomographic analyses of upcoming deep galaxy surveys.

## 4.2 Acoustic Peaks

The first three acoustic peaks are clearly resolved by the current temperature-anisotropy power spectrum. Corresponding oscillations are also apparent in the  $TE$  cross-correlation data and, at lower significance, in the  $EE$  power spectrum. For adiabatic models, the positions of the peaks are at the extrema of a cosine oscillation, giving  $l \approx n\pi d_A(r_*)/r_s$  where  $r_s \equiv \int_0^{\eta_*} c_s d\eta$  is the sound horizon at last scattering. The peak positions thus depend on the physical densities in matter  $\Omega_m h^2$  and baryons  $\Omega_b h^2$  through the sound horizon, and additionally through curvature and dark energy properties from the angular diameter distance. The same physics that gives rise to acoustic peaks in the CMB should produce oscillations in the matter power spectrum. These baryon oscillations were first detected in early 2005 in the clustering of the SDSS luminous red galaxy sample (Eisenstein et al 2005) and in the 2dF galaxy redshift sample (Cole et al 2005). Observing the connection between the fluctuations that produced the CMB anisotropies and those responsible for large-scale structure is an important test of the structure formation paradigm.

The relative heights of the acoustic peaks are influenced by baryon inertia, grav-



itational driving and photon diffusion. Baryons reduce the ratio of pressure to energy density in the plasma, shifting the midpoint of the oscillations to higher over-densities:  $-(1 + R)\psi$ . For adiabatic oscillations this enhances the 1st, 3rd etc. (compressional) peaks over the 2nd, 4th etc. An additional effect comes from the gravitational driving term in equation (4) which initially resonantly drives the acoustic oscillations for the short wavelength modes that underwent oscillation during radiation domination. Increasing the matter density shifts matter-radiation equality to earlier times and the resonance is less effective for the low-order acoustic peaks. In combination, these two effects have allowed accurate measurements of the matter and baryon densities from the morphology of the acoustic peaks. From the three-year WMAP data alone,  $\Omega_b h^2 = 0.0223_{-0.0009}^{+0.0007}$  and  $\Omega_m h^2 = 0.127_{-0.01}^{+0.007}$  in flat,  $\Lambda$ CDM models (Spergel et al 2006). The baryon density implies a baryon-to-photon ratio  $(6.10 \pm 0.2) \times 10^{-10}$  and predicts abundances for primordial deuterium,  $^3\text{He}$  and  $^4\text{He}$  that are consistent with observations. There is some tension between the low matter density favoured by WMAP3 and that favoured by tracers of large-scale structure, most notably weak gravitational lensing (Spergel et al 2006). Better measurements of the third and higher peaks will be very helpful here, and we look forward to sub-percent level precision in the determination of densities with the future Planck data<sup>3</sup>.

With the matter and baryon densities fixed by the morphology of the acoustic peaks, the acoustic oscillations become a standard ruler with which to measure  $d_A(r_*)$ , determined to be  $13.7 \pm 0.5$  Gpc (Spergel et al 2003). The angular diameter distance depends on the Hubble parameter  $H(z)$  and hence the composition of the universe. The dark energy model, curvature and sub-eV neutrino masses have no effect on the pre-recombination universe and they only affect the CMB through  $d_A(r_*)$  and their large-scale clustering through the late-time ISW effect. The discriminatory power of the latter is limited by cosmic variance leading to the *geometric degeneracy* between curvature and dark energy (Efstathiou & Bond 1999). For example, closed models with no dark energy fit the WMAP data but imply a low Hubble constant and  $\Omega_m h$  in conflict with other datasets. Using the Hubble Space Telescope (HST) measurement of  $H_0$ , WMAP3 constrains the spatial sections of the universe to be very close to flat:  $\Omega_K = -0.003_{-0.017}^{+0.013}$  and  $\Omega_\Lambda = 0.78_{-0.058}^{+0.035}$  for cosmological constant models (Spergel et al 2006).

### 4.3 Damping Tail and Photon Diffusion

The acoustic oscillations in the photon-baryon plasma are exponentially damped at last scattering on comoving scales  $\lesssim 30$  Mpc due to photon diffusion (Silk 1968). Furthermore, last scattering is not perfectly sharp: photons last scattered around recombination within a shell of thickness  $\sim 80$  Mpc, and line of sight averaging through this shell also washes out anisotropy from small-scale fluctuations. We thus expect an exponential ‘damping tail’ in the temperature spectrum and this is seen

---

<sup>3</sup><http://www.rssd.esa.int/index.php?project=Planck>

in the ground and balloon-based data in the left plot in Fig. 4.

On scales  $l > 2000$ , the CBI, operating around 30 GHz, sees power in excess of that expected from the primary anisotropies at the  $3\sigma$  level (Bond et al 2005). An excess is also seen at smaller angular scales (centred on  $l \sim 5000$ ) with the BIMA array operating at 28.5 GHz (Dawson et al 2006). Both analyses exclude point-source contamination as the source of the excess, suggesting instead that they are seeing a secondary contribution to the anisotropy from Compton up-scattering of CMB photons off hot gas in unresolved distant galaxy clusters. This explanation in terms of the Sunyaev-Zel'dovich (SZ) effect (Sunyaev & Zeldovich 1972) favours a variance in the matter over-density  $\sigma_8 \approx 1$  (with  $1\sigma$  errors at the 20% level), on the high side compared to inferences from current CMB and large-scale structure data (Spergel et al 2006). Optical follow-up of the BIMA fields shows no (anti-)correlation between galaxy over-densities and the anisotropy images, but the image statistics are consistent with SZ simulations. Data from the several high-resolution CMB experiments that will soon be operational should identify a definitive source for this excess small-scale power.

#### 4.4 *E*-mode Polarization and *TE* Cross-Correlation

Current measurements of the *E*-mode polarization power spectrum and the cross-correlation with the temperature anisotropies are fully consistent with predictions based on the best-fit adiabatic model to the temperature anisotropies. This is an important test of the structure formation model: the polarization mainly reflects the plasma bulk velocities around recombination and these are consistent, via the continuity equation, with the density fluctuations that mostly seed the temperature anisotropies.

Apart from constraints on the reionization optical depth from large-angle polarization data (see Sec. 4.5), the power of the current polarization data for constraining parameters in adiabatic,  $\Lambda$ CDM models is rather limited. More important are the qualitative conclusions that we can draw from the data:

- The well-defined oscillations in  $C_l^{TE}$  further support the phase coherence of the primordial fluctuations, i.e. all modes with a given wavenumber oscillate in phase. This is a firm prediction of inflation models since then the fluctuations are produced in the growing mode and evolve passively, but is at odds with defect models.
- The (anti-)correlation between the polarization and temperature on degree scales (see Fig. 4) is evidence for fluctuations at last scattering that are outside the Hubble radius and are adiabatic (Peiris et al 2003). This is more direct, model-independent evidence for such fluctuations than from the temperature anisotropies since the latter could have been produced on these scales gravitationally all along the line of sight.
- The peak positions in polarization, as for the temperature, are in the correct

locations for adiabatic initial conditions. Pre-WMAP3 analyses, combining CMB temperature and polarization with large-scale structure and nucleosynthesis priors on the baryon density, limit the contribution from isocurvature initial conditions to the CMB power to be less than 30%, allowing for the most general correlated initial conditions (Dunkley et al 2005).

- That  $E$ -mode power peaks at the minima of the temperature power spectrum increases our confidence that the primordial power spectrum is a smooth function with no features ‘hiding’ on scales that reach a mid-point of their acoustic oscillation at last scattering (and so contribute very little to the temperature anisotropies).

#### 4.5 Large-Angle Polarization from Reionization

The large-angle polarization generated by re-scattering at reionization was first seen in the  $TE$  correlation in the first-year WMAP data (Kogut et al 2003). This provided a broad constraint on the optical depth with mean  $\tau = 0.17$  and prompted a flurry of theoretical activity to explain such early reionization. With the full polarization analysis of the three-year release (Page et al 2006), the reionization signal can be seen in the large-angle  $C_l^E$  spectrum (see the insert in the bottom right plot in Fig. 4). To obtain this spectrum required aggressive cleaning of Galactic foregrounds, using the 22.5-GHz (K-band) channel as a template for polarized synchrotron emission and a model for the contribution of polarized thermal dust emission, as well as a careful treatment of correlated noise in the noise-dominated polarization maps. However, the observation that the  $B$ -mode spectrum from the same analysis is consistent with zero suggests that residual foreground contamination is under control. On the basis of the  $EE$  spectrum alone, the WMAP team find  $\tau = 0.10 \pm 0.03$ , considerably lower than the best-fit to the one-year  $TE$  spectrum. The value from the improved three-year analysis sits much more comfortably with astrophysical reionization models.

### 5. CMB Constraints on Inflation

Inflation is a posited period of accelerated expansion in the early universe. It was originally proposed as a solution to a number of now-classic problems with Friedmann cosmologies, such as why the three-geometry is now so close to Euclidean and why the CMB temperature is so uniform given that points at last scattering subtending more than one degree today should never have been in causal contact (Guth 1981). In the inflationary picture, the observable universe is believed to derive from a small, causally-connected region that was inflated by at least 60 e-folds during a phase of accelerated expansion. One mechanism to realise inflation, which requires a violation of the weak energy condition, is with a scalar field  $\phi$  — the inflaton — evolving slowly over a flat part of its interaction potential  $V(\phi)$ . It has proved

difficult to realise inflation from (fundamental) field theory, and this has led to a plethora of phenomenological models in the literature. String-inspired approaches, in which the inflaton may emerge as one of the moduli fields in the low-energy effective theory are also being actively pursued, e.g. Kachru et al (2003).

## 5.1 Inflationary Power Spectra

Inflation naturally predicts a universe that is very close to flat, consistent with the observed positions of the CMB acoustic peaks as discussed in Sec. 4. Significantly, it also naturally provides a causal mechanism for generating initial curvature fluctuations (Bardeen, Steinhardt & Turner 1983) and gravitational waves (Starobinskii 1979) with almost scale-invariant, power-law spectra. The mechanism is an application of semi-classical quantum gravity, in which the perturbations in the inflaton field and metric fluctuations are quantised on a classical background that is close to de Sitter. Since the physical wavelength of a mode gets pushed outside the Hubble radius by the accelerated expansion, vacuum fluctuations initially deep inside the Hubble radius are stretched to cosmological scales and amplified during inflation. The spectra of the curvature perturbations and gravity waves can be approximated as power laws over the range of scales relevant for cosmology:

$$\mathcal{P}_{\mathcal{R}} \approx A_s (k/k_0)^{n_s-1} \quad , \quad \mathcal{P}_h \approx A_t (k/k_0)^{n_t} \quad , \quad (6)$$

where the amplitudes and spectral indices are given by [see e.g. Lidsey et al (1997) and references therein]

$$A_s = \frac{H^2}{\pi \epsilon m_{\text{Pl}}^2} \quad , \quad n_s - 1 = -4\epsilon + 2\eta \quad , \quad A_t \equiv r A_s = \frac{16H^2}{\pi m_{\text{Pl}}^2} \quad , \quad n_t = -2\epsilon \quad . \quad (7)$$

Here,  $H$  is the Hubble parameter during inflation evaluated when the mode  $k_0$  exits the Hubble radius, i.e. when  $k_0 = aH$ , and  $\epsilon$  and  $\eta$  are (Hubble) slow-roll parameters that depend on the evolution of  $H$  through inflation. The potential energy dominates the stress-energy of the scalar field during inflation, and in this limit  $H$ ,  $\epsilon$  and  $\eta$  are related to the potential  $V(\phi)$  by

$$H^2 \approx \frac{8\pi}{3m_{\text{Pl}}^2} V \quad , \quad \epsilon \approx \frac{m_{\text{Pl}}^2}{16\pi} \left( \frac{V'}{V} \right)^2 \quad , \quad \eta \approx \frac{m_{\text{Pl}}^2}{8\pi} \left[ \frac{V''}{V} - \frac{1}{2} \left( \frac{V'}{V} \right)^2 \right] \quad , \quad (8)$$

where primes denote derivatives with respect to the field  $\phi$ . Equations (7) and (8) imply that the power spectrum of gravitational waves from slow-roll inflation depends only the energy density  $V$ . This is often expressed in terms of an *energy scale of inflation*  $E_{\text{inf}} = V^{1/4}$ , which gives a tensor-to-scalar ratio

$$r = 8 \times 10^{-3} (E_{\text{inf}}/10^{16} \text{ GeV})^4 \quad (9)$$

for a scalar amplitude  $A_s = 2.36 \times 10^{-9}$ . The four observables,  $A_s$ ,  $A_t$ ,  $n_s$  and  $n_t$  are not independent since they derive from three parameters,  $H$ ,  $\epsilon$  and  $\eta$ . This

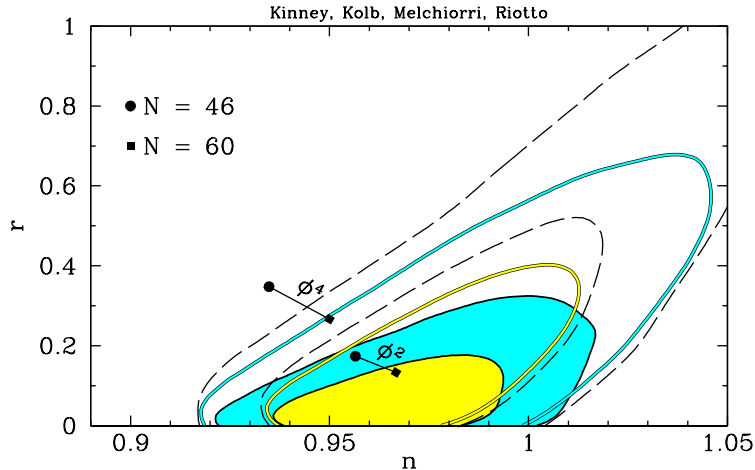


Figure 5. Constraints in the  $r$ - $n_s$  plane for models with no running from Kinney et al (2006). Blue contours are 68% confidence regions and yellow are 95%. The filled contours are from combining WMAP3 and the SDSS galaxy survey; open are with WMAP3 alone. These results assume the HST prior on  $H_0$ ; dropping this prior gives the dashed contours. The predictions for  $V \propto \phi^2$  and  $\phi^4$  are shown assuming that modes with  $k = 0.002 \text{ Mpc}^{-1}$  left the Hubble radius between 46 and 60 e-folds before the end of inflation.

results in the leading-order slow-roll consistency relation  $r = -8n_t$ . Verifying this observationally would be a remarkable triumph for inflation, but the prospects are poor even after accounting for the long lever-arm that a combination of CMB and direct detections could provide (Smith, Peiris & Cooray 2006).

Constraints in the  $r$ - $n_s$  plane from WMAP3 and the SDSS galaxy survey are shown in Fig. 5, taken from Kinney et al (2006). The point  $r = 0$  and  $n_s = 1$  corresponds to inflation occurring at low energy with essentially no evolution in  $H$  (and hence a very flat potential); the gravitational waves are negligible and the curvature fluctuations have no preferred scale. This *Harrison-Zel'dovich* spectrum is clearly disfavoured by the data, but is not yet excluded at the 95% level. Attempts to pin down  $n_s$  with current CMB temperature data are still hampered by a degeneracy between  $n_s$ ,  $A_s$ , the reionization optical depth  $\tau$  and the baryon density (Lewis 2006). The WMAP3 measurement of  $\tau$  from large-angle polarization helps considerably in breaking this degeneracy, and leads to a marginalised constraint of  $n_s = 0.987^{+0.019}_{-0.037}$  in inflation-inspired models (Spergel et al 2006). The 95% upper limit on the tensor-to-scalar ratio from WMAP3 and SDDS is 0.28 for power-law spectra, thus limiting the inflationary energy scale  $E_{\text{inf}} < 2.4 \times 10^{16} \text{ GeV}$ . We see from Fig. 5 that large-field models with monomial potentials  $V(\phi) \propto \phi^p$  are now excluded at high significance for  $p \geq 4$ .

Slow-roll inflation predicts that any running of the spectral indices with scale should be second-order in the slow-roll parameters, i.e.  $O[(n_s - 1)^2]$ . The CMB alone provides a rather limited lever-arm for measuring running, with current data having very little constraining power for  $k > 0.05 \text{ Mpc}^{-1}$  (corresponding to  $l \sim 700$ ).

However, there is persistent, though not yet compelling, evidence for running from the CMB: WMAP3 alone gives  $dn_s/d\ln k = -0.102^{+0.05}_{-0.043}$  (Spergel et al 2006), allowing for gravitational waves. Running near this mean value would be problematic for slow-roll inflation models. The tendency for the CMB to favour large negative running is driven by the large-angle ( $l \lesssim 15$ ) temperature data. A more definitive assessment of running must await independent verification of the large-scale spectrum from Planck and improved small-scale data from a combination of Planck and further ground-based observations. The current evidence for running weakens considerably when small-scale data from the Lyman- $\alpha$  forest (i.e. absorption lines in quasar spectra due to neutral hydrogen in the intergalactic medium) is included (Seljak, Slosar & McDonald 2006; Viel, Haehnelt & Lewis 2006). The Ly- $\alpha$  data probes the quasi-linear fluctuations on  $\sim$  Mpc scales at redshifts around 3, and is sensitive to the amplitude and slope of the matter power spectrum at these redshifts and scales. There is currently some tension between the amplitudes inferred from Ly- $\alpha$  and CMB, and this is worsened by inclusion of the negative running favoured by the CMB.

### 5.3 Non-Gaussianity and Inflation

There are further predictions of slow-roll inflation that are amenable to observational tests. The fluctuations from single-field models should be adiabatic and any departures from Gaussian statistics should be unobservably small. Gaussianity follows, in part, from the requirement of a flat potential and hence small self-interactions if inflation is to happen [see Bartolo et al (2004) for a recent review]. However, adiabaticity and Gaussianity can be violated in models with several scalar fields. An example of the latter is the curvaton model (Lyth & Wands 2002), which can produce a large correlated isocurvature mode and observably-large non-Gaussianity if the curvaton field decays before its energy density dominates that of radiation. As we have already noted, current data do allow a sizeable isocurvature fraction, but this is not favoured. In many models, the non-Gaussian curvature perturbation can be written as the sum of a Gaussian part plus the square of a Gaussian: symbolically

$$\mathcal{R} = \mathcal{R}_G + f_{\text{NL}}^{\mathcal{R}}(\mathcal{R}_G^2 - \langle \mathcal{R}_G^2 \rangle), \quad (10)$$

where, in general,  $f_{\text{NL}}^{\mathcal{R}}$  is scale-dependent and the quadratic part is a convolution. Single-field slow-roll inflation predicts  $f_{\text{NL}}^{\mathcal{R}} \sim O(\epsilon)$  (Maldacena 2003), but it can be much higher in alternative models. Observational constraints are usually expressed in terms of the  $f_{\text{NL}}$  appropriate to the gravitational potential  $\psi$  at last scattering. For  $f_{\text{NL}}^{\mathcal{R}} \gg 1$ , we have  $f_{\text{NL}} \approx -5f_{\text{NL}}^{\mathcal{R}}/3$  since  $O(1)$  non-linear corrections in the relation of the curvature to metric perturbation can then be ignored. The best constraints on a scale-independent  $f_{\text{NL}}$  are from an analysis of the three-point function of the three-year WMAP maps:  $-54 < f_{\text{NL}} < 114$  at 95% confidence (Spergel et al 2006). Planck data should have sensitivity down to  $f_{\text{NL}} \sim 5$  (Komatsu & Spergel 2001), but this is still too large to expect to see anything in simple inflation models.

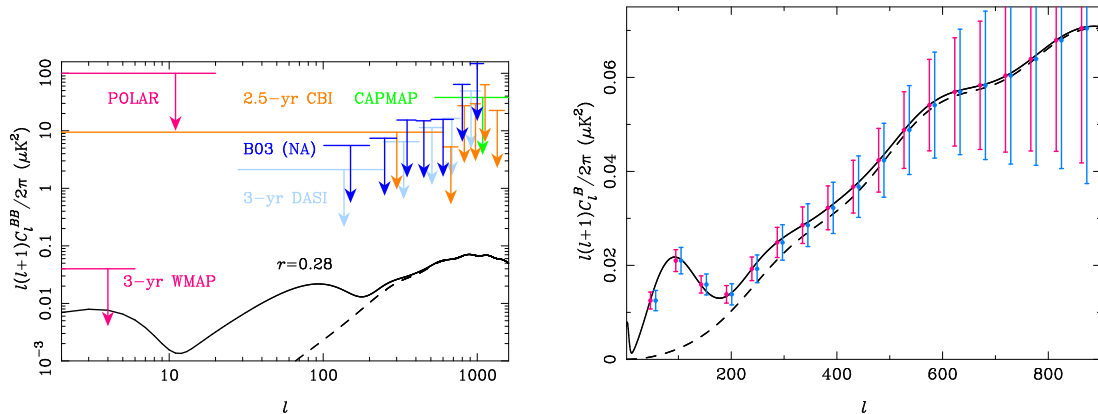


*Figure 6.* Left: current 95% upper limits on the  $B$ -mode polarization power spectrum. The solid line is the theoretical prediction for a tensor-to-scalar ratio  $r = 0.28$  — the current 95% limit from the temperature power spectrum and galaxy clustering (Spergel et al 2006) — while the dotted line is the contribution from weak gravitational lensing. Right: error forecasts for Clover after a two-year campaign observing  $1000 \text{ deg}^2$  divided between four equal-area fields. Blue error bars properly account for  $E$ - $B$  mixing effects due to the finite sky coverage while magenta ignore this. The tensor-to-scalar ratio is again  $r = 0.28$ .

## 6. Searching for Gravity Waves with the CMB

A detection of a Gaussian-distributed background of gravitational waves with cosmological wavelengths and a nearly scale-invariant (but red) spectrum would be seen by many as compelling evidence that inflation occurred. The amplitude of this background is directly related to the energy scale of inflation, and the near scale-invariance follows from the slow decrease in the Hubble parameter during inflation. Of course, a non-detection would not rule out inflation having happened at a low enough energy, but, importantly, a detection would rule out some alternative theories for the generation of the curvature perturbation, such as the cyclic model (Steinhardt & Turok 2002), that predict negligible gravity waves. The large-angle  $B$  mode of CMB polarization is a promising observable with which to search for the imprint of gravity waves since a detection would not be confused by linear curvature perturbations.

In Fig. 6 we show a compilation of current direct upper limits on the  $B$ -mode power spectrum. The solid curve is the theoretical spectrum, including the contribution from weak gravitational lensing, for  $r = 0.28$  — the 95% upper limit inferred from WMAP3 temperature and  $E$ -mode data and SDSS galaxy clustering (Spergel et al 2006). Clearly, the direct measurements are not yet competitive, with at least a factor ten improvement in sensitivity required. The  $2\sigma$  limit to determining  $r$  from ideal CMB temperature observations is 0.14 and this improves to 0.04 with  $E$ -mode data. Although the WMAP temperature data is already cosmic-variance limited on scales where gravity waves contribute, the constraints on  $r$  are considerably worse than  $r = 0.14$  due to the uncertainties in other cosmological parameters. In principle,  $B$ -mode measurements of  $r$  can do much better as they are limited only by how well the lensing signal can be subtracted. Lensing reconstruction methods based on

the non-Gaussian action of lensing on the CMB have been proposed, e.g. Hu (2001), and with the most optimal methods  $r \sim 10^{-6}$  may be achievable (Seljak & Hirata 2003). In practice, astrophysical foregrounds and instrumental systematic effects are likely to be a more significant obstacle.

A number of groups are now designing and constructing a new generation of CMB polarimeters that aim to be sensitive down to  $r \sim 0.01$ . These should be reporting data within the next five years, a timescale similar to the Planck satellite. The constraint  $r < 0.28$  gives an r.m.s. gravity wave contribution  $< 200$  nK to  $B$ -mode polarization. Detecting such signals requires instruments with many hundreds, or even thousands, of detectors, and demands exquisite control of instrumental effects and broad frequency coverage to deal with polarized Galactic foreground emission. With the exception of SPIDER, which will aim to survey around half of the sky, the surveys will each target small sky areas ( $\lesssim 1000$  deg<sup>2</sup>) in regions of low foreground emission in total intensity. Despite this, removing foregrounds to the 10% level will likely be required to see a  $B$ -mode signal at  $r = 0.01$ . As an example of a next-generation instrument, we show in Fig. 6 projected errors on the  $B$ -mode power spectrum from the UK-led Clover experiment. Clover will have over 1200 superconducting detectors distributed over three scaled telescopes centred on 97, 145 and 225 GHz, each with better than 10-arcmin resolution. The instrument is planned to be deployed at the Chajnantor Observatory, Chile. The error forecasts in Fig. 6 are for a tensor-to-scalar ratio  $r = 0.28$  for direct comparison with the adjacent plot of current upper limits. However, the Clover survey is optimised for smaller  $r \sim 0.01$ , and is designed to be limited on large scales by sample variance of the lens-induced  $B$  modes after two years of operation.

## 7. Other Physics in the CMB Fluctuations

Within the  $\Lambda$ CDM model, the major remaining CMB milestones are the detection of gravitational secondary effects (weak lensing and the non-linear ISW effect from collapsing structures), various scattering secondary effects from bulk velocities around and after the epoch of reionization, and the detection of  $B$ -mode polarization and (possibly) gravitational waves. A number of deep surveys at arcminute resolution will soon commence to study the temperature anisotropies at high  $l$ . Their main goal is to characterise the scattering secondaries, and hence learn more about the reionization history and morphology, and to detect the gravitational lensing effect in the temperature anisotropies. At the same time, high-sensitivity polarization surveys are being undertaken and these should also provide further valuable information on the weak-lensing effect. From the viewpoint of fundamental physics, the main interest in such small-scale observations is the possibility of using CMB lensing to determine neutrino masses and further constrain the dark-energy model. However, we should also be mindful of the possibility of serendipitous discovery of other physics in the small-scale CMB fields, such as the imprint of cosmic strings or primordial magnetic fields. We now discuss some of these briefly.

Cosmology has the potential to place constraints on the absolute neutrinos masses



rather than the (squared) differences from neutrino oscillations [see Lesgourgues & Pastor (2006) for a recent review]. The current constraint on the sum of neutrino masses from CMB, galaxy clustering and Lyman- $\alpha$  forest data is  $\sum m_\nu < 0.17$  eV at 95% confidence (Seljak et al 2006). The implied sub-eV masses mean neutrinos are relativistic at recombination and their effect on the CMB is limited to late times. Changes they induce in the angular diameter distance are degenerate with dark energy and so, to constrain masses from the CMB alone, we need to look to gravitational lensing. Non-relativistic massive neutrinos increase the expansion rate over massless one impeding the growth of structure. This effect is cancelled on scales larger than the neutrino comoving Jeans' length (which decreases in time and is inversely proportional to the mass) by neutrino clustering, but on smaller scales the growth of fluctuations in the matter density is slowed. It is this suppression that allows the energy density (or sum of masses) of neutrinos to be constrained by small-scale tracers of matter clustering. The effect of neutrino masses on the power spectrum of the lensing deflections is scale dependent: no effect at low  $l$  but a reduction in power at high  $l$ . To exploit the effects of neutrino physics in CMB lensing, one must first attempt to reconstruct the underlying lensing deflection field from the lensed CMB fields. An accurate reconstruction requires high resolution and is greatly helped by polarization measurements once the sensitivity is high enough to image lens-induced  $B$  modes (Hu & Okamoto 2001; Seljak & Hirata 2003). Assuming a normal hierarchy of neutrino masses with two essentially massless<sup>4</sup>, Kaplinghat, Knox & Song (2003) estimated that the mass of the third should be measurable to an accuracy of 0.04 eV with a future polarization satellite mission. Errors of this magnitude are comparable to what should be achievable in the future with galaxy lensing, but with quite different potential systematic effects. It is an interesting result since atmospheric neutrino oscillations then imply that a detection of mass with the CMB *must* be possible at the  $1\sigma$  level. Of course, the significance will be higher if the lightest neutrinos are not massless, or in the inverted hierarchy. Note that the latter is on the verge of being ruled out with the current cosmological constraints (Seljak et al 2006). It is also interesting to question whether CMB lensing will be able to tell us anything about individual masses rather than their sum? Taking differences from oscillation data at face value, the answer appears to be that dropping the assumption of degenerate masses would produce an improved fit to an idealised, cosmic-variance-limited reconstruction of the lensing power spectrum if  $\sum m_\nu < 0.1$  eV (Slosar 2006). However, attempting to measure the mass differences with no prior from atmospheric oscillations is not possible because of degeneracies with other parameters and these severely degrade ones ability to measure  $\sum m_\nu$  without mass priors.

The details of the dark-energy sector affect the primary CMB anisotropies only through the angular diameter distance and the late-time ISW effect. Using the former is plagued by degeneracies while the latter is hampered by cosmic variance. The effect of dark energy on CMB lensing is felt almost exclusively through the change in the expansion rate which is independent of scale. The different scale

---

<sup>4</sup>This combination has the smallest possible neutrino energy density and hence cosmological effect.

dependences from dark energy (say to changes in the equation of state parameter  $w = p/\rho$ ) and massive neutrinos should allow them to be measured separately with the lensed CMB. Kaplinghat et al (2003) find a marginalised  $1\sigma$  error on  $w$  of 0.18 from a future polarization satellite. Of course, tomography proper is not possible with the fixed source plane of the CMB (i.e. last scattering), and the CMB constraints on dark energy will not be competitive with future galaxy lensing and clustering (via baryon oscillations) surveys.

A significant feature of recent attempts to realise inflation in string/M-theory cosmology is the recognition that (local) cosmic strings may be produced generically at the end of brane inflation (Sarangi & Tye 2002). The details of the strings network (such as the spectrum of tensions and inter-commutation rates) depend on the details of the brane scenario, but the tensions  $G\mu/c^4$  plausibly exceed  $10^{-11}$ . Cosmic strings leave an imprint in the CMB temperature anisotropies due to string wakes stirring up the plasma prior to recombination, and from the integrated effect of rapidly moving strings crossing the line of sight (Kaiser & Stebbins 1984). Current data limits the contribution of local strings to the temperature power spectrum to be  $\lesssim 10\%$ , corresponding to  $G\mu/c^4 < 2.7 \times 10^{-7}$  (Seljak et al 2006). Future high-resolution temperature data should improve this bound on the tension further, and searches for stringy non-Gaussian imprints in CMB maps should also help. As with the search for inflationary gravitational waves,  $B$ -mode polarization may prove to be the most promising observable for constraining strings. String networks excite scalar, vector and tensor perturbations and the latter two lead to  $B$ -mode polarization from the epoch of recombination and reionization. Many brane-inflation models predict a negligible gravity wave production *during* inflation in which case strings should be the dominant primordial source of  $B$ -mode polarization. Seljak & Slosar (2006) argue that  $B$ -mode measurements with a future polarization satellite may improve on current string constraints by an order of magnitude. The string signal peaks around  $l \sim 1000$  and so the hope is that observations covering a range of scales should be able to separate it from primordial gravity waves and the lensing signal. However, further work is required to extend and test lensing reconstruction methods in the presence of a possible non-Gaussian string signal.

Finally, we note that there are statistically-significant anomalies in the large-angle temperature anisotropies, as imaged by COBE (Smoot 1992) and WMAP (Hinshaw 2003), that may signal departures from rotational invariance and/or Gaussianity; for a recent review and WMAP3 analysis, see Copi et al (2006) and references therein. Arguably most significantly, the  $l \leq 6$  multipoles seem to favour a preferred axis about which they maximise the power concentrated in a single  $m$  mode (Land & Magueijo 2005). There are also significant correlations of the quadrupole and octupole ( $l = 3$ ) with the ecliptic plane and the direction of the equinoxes and/or CMB dipole (Copi et al 2006). The significance of these anomalies is still under debate, as is their possible explanation. Suggestions include unidentified instrumental effects, residual foreground contamination, and effects of the local universe (Vale 2005), although it appears unlikely that the last two can be responsible (Cooray & Seto 2005). There have also been a number of suggestions that the large-angle anomalies may have a more fundamental origin, such as a topologically small universe (de

Oliveira-Costa et al 2004) or non-fluid dark energy (Battye & Moss 2006). Independent verification with the Planck data and improved analyses of further years of WMAP data should help with tracking down the source of these large-angle effects<sup>5</sup>.

## 8. Summary

Many of the bold predictions of CMB physics have now been impressively verified with a large number of independent observations. The large-scale Sachs-Wolfe effect, acoustic peak structure, damping tail, late-time integrated Sachs-Wolfe effect,  $E$ -mode polarization and the effect of reionization have all been detected. The large-scale anisotropies and the first three acoustic peaks have now been measured accurately and have yielded impressive constraints on cosmological parameters. The data is consistent with a very simple cosmological model with adiabatic primordial fluctuations, with an almost scale-free spectrum, evolving passively in a spatially-flat,  $\Lambda$ CDM universe.

Inflation continues to stand up to exacting comparisons with both CMB and tracers of matter clustering. Evidence for dynamics during inflation is emerging, most notably from the recent third-year WMAP data: models with scale-invariant curvature perturbations and no gravity waves are on the brink of being ruled out at 95% confidence. There are hints of a run in the spectral index in current CMB data at a level that would be problematic for many inflation models, but this is not corroborated by probes of the matter power spectrum on small scales (the Lyman- $\alpha$  forest). In the near future we can expect better measurements of the third acoustic peak in the temperature anisotropies and beyond. With Planck we can expect a per-cent level determination of the spectral index of curvature perturbations and a much more definitive assessment of running and any potential conflict with the small-scale matter power spectrum.

We look forward to improvements in  $E$ -mode polarization data and the better constraints this will bring on non-standard cosmological models such as those with a significant contribution from isocurvature fluctuations. On a similar timescale, a new generation of small-scale temperature experiments should constrain further the reionization history and its morphology, and detect the effect of weak gravitational lensing by large-scale structure in the CMB. Looking a little further ahead, a new generation of high-sensitivity polarization-capable instruments have the ambition of detecting the imprint of gravitational waves from inflation. They should be sensitive down to tensor-to-scalar ratios  $r \sim 0.01$  — corresponding to an energy scale of inflation around  $1.0 \times 10^{16}$  GeV — and will place tight constraints on inflation models. There is also exciting secondary science that can be done with these instruments, such as lensing reconstruction which brings with it the promise of competitive constraints on neutrino masses from the CMB alone. Finally, there is always the hope of serendipitous discovery, such as the non-Gaussian signature of cosmic strings,

---

<sup>5</sup>The first-year WMAP data was already signal-dominated on large angular scales so further integration helps not by improving the signal-to-noise but by bettering our understanding of instrumental and foreground effects.

perhaps produced at the end of brane inflation, in small-scale temperature maps. These continue to be exciting times for CMB research.

## Acknowledgements

AC thanks the Royal Society for a University Research Fellowship, the organisers for the invitation to attend this stimulating workshop and the British Council for sponsoring my attendance. Thanks also to Will Kinney and Bill Jones for permission to include their figures.

## References

- Bardeen, J.M., Steinhardt, P.J., Turner, M.S., 1983, Phys. Rev. D, 28, 679  
Battye, R.A., Moss, A., 2006, arXiv:astro-ph/0602377  
Bartolo, N. et al, 2004, Phys. Rept., 402, 103  
Bennett, C.L. et al, 2003, ApJS, 148, 1  
Bond, J.R. et al, 2005, ApJ, 626, 12  
Bough, S., Crittenden, R., 2004, Nature, 427, 45  
Cabre, A. et al, 2006, arXiv:astro-ph/0603690  
Challinor, A., 2005, in *The Physics of the Early Universe*, E. Papantonopoulos (ed.), Lect. Notes. Phys. 653, 71  
Cole, S. et al, 2005, MNRAS, 362, 505  
Cooray, A., Seto, N., 2005, JCAP, 12, 4  
Copi, C. et al, 2006, arXiv:astro-ph/0605135  
Dawson, K.S. et al, 2006, arXiv:astro-ph/0602413  
Dunkley, J. et al, 2005, Phys. Rev. Lett., 95, 261303  
Eisenstein, D.J. et al, 2005, ApJ, 633, 560  
Efstathiou, G., Bond, J.R., 1999, MNRAS, 304, 75  
Guth, A.H., 1981, Phys. Rev. D, 23, 347  
Hinshaw, G. et al, 1996, ApJL, 464, 17  
Hinshaw, G. et al, 2006, arXiv:astro-ph/0603451  
Hu, W., 2001, ApJL, 557, 79  
Hu, W., 2002, Ann. Phys., 303, 203  
Hu, W., Sugiyama, N., 1995, ApJ, 444, 489  
Hu, W., White, M., 1997, Phys. Rev. D, 56, 596  
Hu, W., Dodelson, S., 2002, Ann. Rev. Astron. Astrophys., 40, 171  
Hu, W., Okamoto, T., 2002, ApJ, 574, 566  
Jones, W.C. et al, 2005, arXiv:astro-ph/0507494  
Kachru, S. et al, 2003, JCAP, 0310, 013  
Kaiser, N., Stebbins, A., 1984, Nature, 310, 391  
Kamionkowski, M., Kosowsky, A., Stebbins, A., 1997, Phys. Rev. D, 55, 7368  
Kaplinghat, M., Knox, L., Song, Y.S., 2003, Phys. Rev. Lett., 91, 241301  
Kinney, W.H. et al, 2006, arXiv:astro-ph/0605338

Kogut, A. et al, 2003, ApJS, 148, 161  
Komatsu, E., Spergel, D.N., 2001, Phys. Rev. D, 63, 063002  
Land, K., Magueijo, J., 2005, Phys. Rev. Lett., 95, 071301  
Lesgourgues, J., Pastor, S., 2006, arXiv:astro-ph/0603494  
Lewis, A., 2006, arXiv:astro-ph/0603753  
Lewis, A., Challinor, A., 2006, Phys. Rept., 429, 1  
Lidsey, J.E. et al, 1997, Rev. Mod. Phys., 69, 373  
Lyth, D.H., Wands, D., 2002, Phys. Lett. B, 524, 5  
Maldacena, J., 2003, J. High Energy Phys., 5, 13  
Mather, J.C. et al, 1994, ApJ, 420, 439  
de Oliveira-Costa, A. et al, 2004, Phys. Rev. D, 69, 063516  
Page, L. et al, 2006, arXiv:astro-ph/0603450  
Peiris, H.V. et al, 2003, ApJS, 148, 213  
Rees, M.J., 1968, ApJL, 153, 1  
Sachs, R., Wolfe, A., 1967, ApJ, 147, 735  
Sarangi, S., Tye, S.H.H., 2002, Phys. Lett. B, 536, 185  
Seljak, U., Hirata, C.M., 2004, Phys. Rev. D, 69, 043005  
Seljak, U., Slosar, A., 2006, arXiv:astro-ph/0604143  
Seljak, U., Slosar, A., McDonald, P., 2006, arXiv:astro-ph/0604335  
Silk, J., 1968, ApJ, 151, 459  
Slosar, A., 2006, arXiv:astro-ph/0602133  
Smith, T.L., Peiris, H.V., Cooray, A., 2006, arXiv:astro-ph/0602137  
Smoot, G.F. et al, 1992, ApJL, 396, 1  
Spergel, D.N. et al, 2003, ApJS, 148, 175  
Spergel, D.N. et al, 2006, arXiv:astro-ph/0603449  
Starobinskii, A.A., 1979, JETP Lett., 30, 682  
Steinhardt, P.J., Turok, N., 2002, Science, 296, 1436  
Sunyaev, R.A., Zeldovich, Y.B., 1972, Comm. Astrophys. Space Phys., 4, 173  
Vale, C., 2005, arXiv:astro-ph/0509039  
Viel, M., Haehnelt, M.G., Lewis, A., 2006, arXiv:astro-ph/0604310  
Zaldarriaga, M., 1997, Phys. Rev. D, 55, 1822  
Zaldarriaga, M., Seljak U., 1996, Phys. Rev. D, 55, 1830  
Zaldarriaga, M., Seljak, U., 1998, Phys. Rev. D, 58, 023003